Renewable-integrated flexible production of energy and methane via re-using existing offshore oil and gas infrastructure

Alirahmi, Seyed Mojtaba; Perrucci, Alessandro; Maschietti, Marco; Qi, Meng; Gençer, Emre; Sin, Gürkan; Yu, Haoshui

Published in:
Journal of Cleaner Production

DOI (link to publication from Publisher):
10.1016/j.jclepro.2023.139125

Publication date:
2023

Document Version
Publisher's PDF, also known as Version of record

Journal of Cleaner Production 426 (2023) 139125

Contents lists available at ScienceDirect

Journal of Cleaner Production

journal homepage: www.elsevier.com/locate/jclepro

Renewable-integrated flexible production of energy and methane via re-using existing offshore oil and gas infrastructure

Seyed Mojtaba Alirahmi [a], Alessandro Perrucci [a], Marco Maschietti [a], Meng Qi [b], Emre Gençer [c], Gürkan Sin [d], Haoshui Yu [a,*]

[a] Department of Chemistry and Bioscience, Aalborg University, Niels Bohrs Vej 8A, Esbjerg, 6700, Denmark
[b] College of Chemistry and Chemical Engineering, China University of Petroleum (East China), Qingdao, 266580, China
[c] MIT Energy Initiative, 77 Massachusetts Avenue, Cambridge, MA, 02139, USA
[d] Process and Systems Engineering Center (PROSYS), Department of Chemical and Biochemical Engineering, Technical University of Denmark, Søltofts Plads 228 A, 2800, Kgs. Lyngby, Denmark

ARTICLE INFO

Handling Editor: Cecilia Maria Villas Bôas de Almeida

Keywords:
Offshore platform repurposing
Offshore wind farm
Carbon capture utilization and storage
Process integration
Allam cycle
Power-to-methane

ABSTRACT

Denmark has been extracting gas and oil from the North Sea since the 1970s. However, Denmark has recently committed to phasing out fossil fuel production by 2050 to meet the climate goals of the Paris Agreement. The decommissioning of the offshore infrastructure is going to be very expensive. Therefore, considering effective ways for its repurposing becomes of great interest. In parallel to this scenario, the energy transition towards renewable and sustainable energy supply has been boosting the construction of offshore wind farms (OWF) in the North Sea. In this context, the integration of OWF with offshore oil and gas (O&G) platforms could result in a better alternative to decommissioning. In this work, a novel zero-carbon emission energy system for both power generation and methane production is proposed. By utilizing surplus electricity from OWF, electrolysis can be used to split water into oxygen and hydrogen, which can be used in the Allam cycle for power generation and methanation according to the Sabatier reaction, respectively. In this novel integrated system, surplus electricity from wind farms, seawater, and CO_2 are converted into controllable electricity, methane, and oxygen. The synthesized methane can be partly stored or exported via existing natural gas pipelines. The portion to be stored/exported is defined as the storage ratio in this study. The integrated system has high flexibility since the Allam cycle and methanation unit can be operated separately or simultaneously. To validate the feasibility of the system, preliminary energy and exergy analysis are performed using Engineering Equation Solver (EES) software. 1% (45 ton/day) of the total daily Danish natural gas consumption is assumed as the baseline for the modeling. If all the synthesized methane is burned in the Allam cycle, 51.34 MW of electricity from wind farms can be transformed into 16.4 MW of controllable electricity. In this scenario, the integrated system can be regarded as an energy storage system, where the round-trip efficiency is about 32%.

1. Introduction

Due to the increasing concern about climate change, decarbonization is gaining significant attention from both academia and industry. One third of the yearly global greenhouse gas emissions are caused by the energy-intensive sector (Bataille et al., 2018). The oil and gas (O&G) industry is one of the largest emission sectors. To meet the climate goals set out in the Paris Agreement, many countries have set up their timeline toward carbon neutrality. Denmark is a leading country in renewable energy and carbon neutrality. As for the O&G industry, the Danish government has recently committed to phasing out fossil fuel production by 2050. Consequently, the offshore O&G infrastructure in the Danish North Sea will have to be decommissioned. However, decommissioning is expected to be very costly, and it is therefore of interest to evaluate if the existing installations can be repurposed to produce energy and/or chemicals from sources other than fossil hydrocarbons in a profitable and environmentally friendly manner.

Among factors hindering the repurposing, space availability in conventional offshore O&G platforms is limited and the power and heat generation relies on a simple gas turbine (GT) cycle, which has lower

* Corresponding author.
E-mail address: hayu@bio.aau.dk (H. Yu).

https://doi.org/10.1016/j.jclepro.2023.139125
Received 10 March 2023; Received in revised form 15 September 2023; Accepted 29 September 2023
Available online 30 September 2023

efficiency and higher environmental impacts compared to modern thermal power plants. In the GT cycle, the waste heat can be recovered by a steam cycle in order to increase efficiency, however the steam cycle has many pieces of auxiliary equipment and a huge Heat Recovery Steam Generator (HRSG) and condenser. Therefore, it is difficult to decrease the size of the steam cycle. One of the major parameters affecting the size of power generation systems is the type of working fluid. Cycles based on supercritical fluids have remarkable advantages from size and efficiency standpoints.

Supercritical carbon dioxide (sCO_2) cycles are specific types of supercritical power plants that use CO_2 as a working fluid and operate at or above critical point. The high density of sCO_2 leads to compact equipment, such as turbomachines, and heat exchangers. The sCO_2 oxy-fuel is a variant of the sCO_2 cycle that uses oxy-fuel combustion as the heat source. Accordingly, sCO_2 oxy-fuel power cycles could be a promising solution with near-zero emissions, simplicity (fewer parts), and higher efficiency (Xie et al., 2023). Since sCO_2 oxy-fuel cycles are operated at high pressure, the sCO_2 density remains high throughout the whole power cycle, compared with steam Rankine cycles, which operate at 1500–2500 kPa, and gas Brayton cycles, which operate at 1500–3000 kPa. Therefore, when the density of sCO_2 rises, the volumetric flow rate decreases, which lead to 10 times smaller turbomachines compared to that of a steam Rankine cycle.

In past decades, multiple oxy-fuel combustion cycles have been proposed including MATIANT cycle (Mathieu and Nihart, 1999), Graz cycle (Sanz et al., 2005), and semi-closed oxy-fuel combustion combined cycle (Bolland and Mathieu, 1998). Recently Allam et al. (2013) recommended a semi-closed oxy-fuel, later called the Allam cycle. This cycle uses the gas produced from oxy-fuel combustion as the working fluid. Rogalev et al. (2021) analyzed and compared the current oxy-fuel cycles. According to the results, the Allam cycle has many advantages over other oxyfuel cycles, such as low installation costs and high electricity efficiency. Scaccabarozzi et al. (2016) obtained some operational conditions to maximize oxy-fuel combustion cycle energy efficiency and proposed further technical and economical optimizations for future studies. The oxy-fuel cycle requires almost pure oxygen stream, which can be derived from an air separation unit (ASU). However, the ASU is a major barrier in terms of energy and cost issues in oxy-fuel combustion power generation.

In parallel to this scenario, offshore wind energy has been growing fast in the last decade. EU offshore wind farms (OWF) produce about 22 GW of electricity, with 77% being located in the North Sea. The capacity of offshore wind energy is expected to expand to 70 GW by 2030 and 112 GW by 2040 (McKenna et al., 2021). The wind is one of the most intermittent energy sources among various renewable energy (Behzadi et al., 2023). The fast ramping and intermittent nature of wind energy generation makes power grid integration challenging (Shabani et al., 2022). Consequently, energy storage technologies are essential to overcome the alternating and fluctuating nature of wind energy (Li et al., 2022). The power-to-X (PtX) concept has a high potential for large-scale and flexible storage of excess wind energy (Wulf et al., 2020). The PtX method has been discussed in recent years as a coupling and energy storage technology. PtX is a method to convert electrical energy into chemical energy. Schaaf et al. (2014) reported that synthetic natural gas (SNG) has a longer discharge time and a higher storage capacity compared to other storage technologies like flywheels and batteries. Besides, analyzing the energy and exergy flows of PtX systems helps in understanding the irreversibility of its components and their environmental performance. The majority of the research on PtX systems has been focused on techno-economic aspects, while only a few investigations comprised the thermodynamics of the CO_2 methanation process. Luo et al. (2017) investigated the exergy efficiency of a power-to-methane (PtM) system consisting of a Sabatier reactor and an electrolyzer. Toro and Sciubba (2018) analyzed the exergy of a CO2 methanation process. According to their findings, a Sabatier conversion yield of 93.48% can be achieved, and PtM has great potential for energy storage.

In PtX processes, oxygen is one of the by-products, which is rarely used in most applications, and often released into the atmosphere or piped into tanks for later use (Thema et al., 2019). Efficient utilization of oxygen could be the key to improving the PtX economic performance (Hermesmann et al., 2021). Hence, using oxygen as an oxidant stream has a huge potential for improving the efficiency of integrated energy systems (IES). On the other hand, the oxygen storage on offshore platforms is challenging due to space limitation. Therefore, in this study, underwater compressed oxygen energy storage (UWCOES) technology is proposed to store oxygen. This idea is motivated by the underwater compressed air energy storage (UWCAES), where excess renewable energy is converted into high pressure air to store energy. There are various suitable conditions for compressed oxygen storage in the maritime environment. In an underwater storage, the compressed oxygen is stored at about the same hydrostatic pressure as the surrounding water, thus the water counteracts the pressure of the compressed oxygen decreasing the cost of the tank (Pimm and Garvey, 2022). There have been no studies on underwater compressed oxygen storage so far. However, some researchers have focused on strengthening the structure and optimizing the UWCAES parameters. Cheung et al. (2014), investigated multi-objective optimization on the UWCAES design parameters. The round-trip efficiency of the proposed system was 68.5% based on their results. Wang et al. (2016) suggested a multi-layer UWCAES system, which was evaluated based on exergy analysis. According to their results, the exergy efficiency ranges from 62 to 81% based on the operational conditions.

Oxy-fuel cycles and offshore platforms are usually studied independently, and their combination is rarely investigated. Designing an offshore platform is practical but challenging because of strict weight and space limitations. In this context, repurposed offshore O&G platforms and offshore wind farms can be integrated to overcome the challenges faced by the offshore industry. As discussed, synergistic integration could lead to both economic and environmental benefits. However, the synergies between the offshore platforms and the offshore wind farms heavily depend on the design of the integrated system. This study proposed a novel integrated system, which can take full advantage of the offshore oil and gas platforms, by re-using substantial parts of the existing facilities, as well as offshore wind farms. The main highlights of the current research are as follows:

- An innovative system to repurpose the offshore oil and gas platforms to produce both electricity and methane without emissions.
- The potential for significant cost savings by avoiding expensive decommissioning of the offshore oil and gas infrastructure.
- An innovative approach to integrate carbon storage and carbon utilization to produce synthetic methane, which is not only an energy carrier but also a critical bulk chemical for the production of carbon-based petrochemicals that enhances the geopolitical independency of countries not producing fossil fuels.
- Underwater compressed oxygen energy storage (UWCOES) coupled with Allam cycle for saving space on repurposed offshore platforms and supplying high purity oxygen to the power cycle.

The present study employs both energy and exergy analysis to comprehensively assess the novel integrated system. To better understand the system's performance, a Grassmann exergy diagram is developed to visualize the exergy rate of each stream and the exergy destruction of each component to identify any bottlenecks in the system. Furthermore, the share of each subsystem on the total exergy destruction is shown using a Chord diagram.

2. System description and scenarios

The novel integrated energy and chemical system re-uses part of the existing offshore O&G infrastructure, while managing the offshore wind

farm intrinsic variability with the increasing installed capacity. The novel integrated system is shown in Fig. 1. It includes offshore wind farms, carbon storage, units for reverse osmosis (RO) desalination, electrolysis, UWCOES, and methanation, as well as an Allam cycle power generation unit. The overall inputs of the system are electricity, either from the grid or dedicated wind farms, carbon dioxide, and seawater, while the overall outputs are methane, oxygen, and dispatchable electricity. The subsystems are interconnected via energy and material streams. A brief overview of each subsystem is provided below.

2.1. Offshore wind farms

The offshore wind industry is a crucial sector in the energy transition for Denmark to reduce greenhouse gas emissions. At present, offshore wind power technology has reached a mature stage and is undergoing large-scale installation (Zhixin et al., 2009). Offshore wind farms generate intermittent and unstable electricity. Managing this intrinsic variability is critical to effectively utilize offshore wind energy. By converting excess energy into chemicals, offshore wind energy production can be expanded and used for large-scale energy storage or the petrochemical industry.

It is here envisaged that OWF in the North Sea will be integrated with the repurposed offshore O&G platforms. These OWF could be connected to the repurposed offshore O&G platform only, in which case the only system output will be methane and oxygen, or they can be connected to the grid as well, in which case electricity on-demand can also be a system output as shown by the purple lines in Fig. 1. If the OWF are connected to the grid, in principle the methanation unit could be placed either offshore or onshore. However, the implementation of the methanation unit offshore, as represented in Fig. 1, has two distinct advantages: (i) keep the gas production far away from the place where people live, thus increasing the social acceptance of large-scale gas and electricity production, due to negligible visual and noise impact; (ii) reuse the existing infrastructure, which includes natural gas dehydration, compression, and piping.

2.2. RO desalination unit

A highly pure water feed is one of the requirements of water electrolysis, which can be produced through different desalination technologies. Since seawater makes up around 96.5% of the world's water resources, research into direct seawater electrolysis for hydrogen generation has been initiated. Direct seawater electrolysis could potentially be used on offshore platforms, where fresh water is not available but there is easy access to seawater and renewable energy sources. However, direct seawater electrolysis is still at an early stage of development. In this study, we consider the desalination of seawater by means of RO, which is an established technology, and based on the results we can conclude if the direct seawater electrolysis deserves further investigation in this proposed system. The seawater in the RO system is pumped by a high-pressure pump (State 1) through membranes where seawater is desalinated (State 2), and the desalinated water is then mixed with recycled water from the methanation unit (State 3) and stored in a tank (State 5).

2.3. Electrolysis process

Electrolysis of water to produce hydrogen and oxygen is the foundation of PtX technologies. Hydrogen produced from the electrolysis process driven by renewable energy is termed as green hydrogen. To produce green hydrogen, electrolyzers are the key equipment in the process. In this study, the polymer-electrolyte-membrane (PEM) technology is adopted for hydrogen production because polymer electrolytes possess high mechanical strength and durability, high oxidative stability, and high conductivity for proton transport. The PEM electrolyzer produces a water-oxygen mixture and hydrogen. The generated oxygen leaves the PEM through the anode (State 8) and after compression (State 11) it is stored in the oxygen bags (State 20). The produced hydrogen leaves the PEM through the cathode (State 7) and then is conveyed to the methanation unit.

As an alternative application, the produced hydrogen from PEM could also be directly used as fuel or injected into the NG pipeline, however with limitations of the volumetric percentage. Pure hydrogen

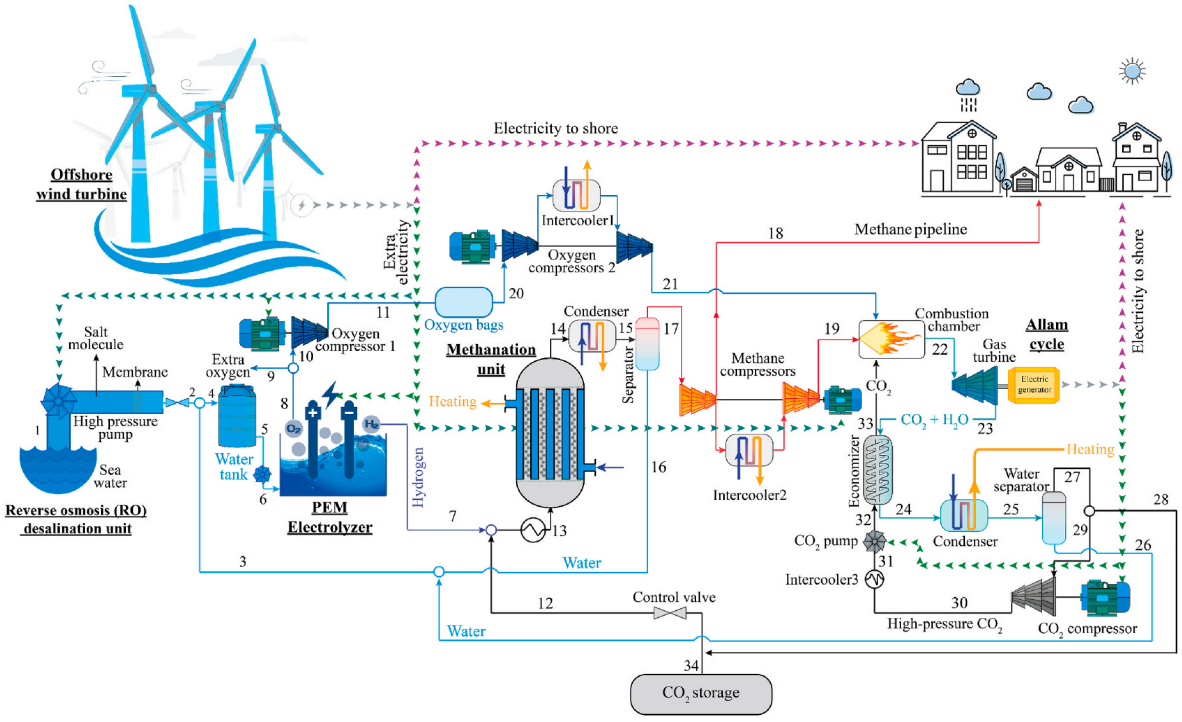

Fig. 1. The process flow diagram of the proposed IES.

can not be injected into the existing NG pipeline because of corrosion issues (Wu et al., 2022) which can pose challenges for aging infrastructure, like the North Sea O&G unless the NG pipelines undergo a requalification process. Therefore, hydrogen is usually blended with NG and thus can be transported by the NG pipeline. Hydrogen-blended natural gas transmission has been demonstrated in many countries using existing pipelines. However, after 2050, offshore platforms do not produce NG anymore. Therefore, the pure hydrogen has to be converted into methane to facilitate transportation in the existing NG pipeline. To convert the hydrogen into methane, a methanation unit has to be configured in the integrated system.

2.4. Methanation unit

To develop carbon capture utilization and storage (CCUS) systems and to convert hydrogen into a transportable product for the existing natural gas pipeline after 2050, the methanation process is adopted in this novel integrated system. CO_2 can be converted into CH_4 via the Sabatier reaction, which is considered a highly attractive approach for the utilization of CO_2 to produce clean and green fuels beyond 2050. In this novel integrated energy system, the hydrogen is converted into methane, which can be conveyed to the existing NG pipeline or burned offshore in the Allam cycle for power generation. H_2 and CO_2 are required for the methanation process. By combining the H_2 produced from the PEM electrolyzer (State 7) with CO_2 from the Allam cycle and/or CO_2 storage (State 12), the methanation unit can produce the CH_4 for the dual use of energy storage or bulk chemical for petrochemical industry.

2.5. Allam cycle

CO_2 is the working fluid in the Allam cycle, which is an oxy-fuel power cycle. Offshore O&G industries are usually powered by a simple GT cycle, which burns NG and emits carbon dioxide into the atmosphere. In contrast, the Allam cycle as an oxy-fuel power cycle is capable of achieving near-zero emissions since the CO_2 can be captured easily in the flue gas. Therefore, the Allam cycle is a more promising future power generation technology. Furthermore, the Allam cycle is much more compact compared with conventional gas turbines, making it ideal for the space and weight constraints of offshore platforms. For the above-mentioned reasons, the Allam cycle is an attractive option for production of electricity in the context of repurposing offshore O&G platforms.

In the combustion chamber of the Allam cycle, high-pressure O_2 (State 21) is mixed with CH_4 (State 19), and recycled sCO_2 (State 33), which has the function of controlling the temperature of the combustion products by dilution. Then the combustion products (sCO_2 + steam) at high pressure and temperature (State 22) enter the turbine to expand and drive the electric generator. The turbine exhausts (State 23), with relatively high temperatures, proceed to the economizer to preheat the recycled sCO_2 (State 32). After that, the combustion products are cooled in the condenser (State 25), where water is separated from the combustion products and recycled (State 26) and the highly pure CO_2 is compressed to the supercritical region (State 30). Before the compression, a portion of the CO_2 is conveyed to the methanation unit (State 28) at a rate equivalent to the rate of CO_2 created during combustion (to maintain a constant mass flow rate). Finally, the recycled sCO2 is pressurized by the pump (State 31) and heated up with the economizer (State 33) prior to the combustion process.

2.6. CO_2 storage system

CCUS is a promising strategy for mitigating climate change. For the past few decades, a Norwegian oil company has demonstrated that carbon capture and storage (CCS) can be used to achieve the climate goals outlined in the Paris Agreement. To ensure safe storage of CO_2, reservoirs with adequate porosity and permeability, as well as thick and impermeable cap rocks, are required. Depleted oil and gas reservoirs can satisfy the above criteria and therefore considered as ideal sites for carbon storage (Schrag, 2009). In the proposed process, the stored CO_2 in the reservoir can be utilized as the raw material for the methanation unit, in line with CCUS concepts.

The abovementioned subsystems are interconnected as illustrated in Fig. 1. However, there are many possible configurations of the integrated system. For instance, the Allam cycle can be removed if the sole objective is to produce methane for export. The ratio of the methane for export to burned methane in the Allam cycle can also be adjusted depending on specific needs. Therefore, multiple scenarios are examined and discussed in the results and discussion section.

3. Thermodynamic and electrochemical modeling

The model of the proposed IES is developed in EES. The energy balance, mass balance, and exergy equations of each subsystem and component are implemented in EES to assess the system performance. This work focuses on a case study of Denmark, where it is assumed that the methanation reactor produces 45 t/day of methane, which represents approx. 1% of Denmark's current natural gas consumption, equivalent to 2.3 billion cubic meters as per 2021 (Statista, 2022). To demonstrate the flexibility of the integrated energy system, the study simulated multiple scenarios by varying the ratio of the synthesized methane for export to the total methane produced in the methanation unit, with values of 0%, 25%, 50%, 75%, and 100% being considered. The remaining synthetic methane is burned in the Allam cycle. The other assumptions used in the modeling of the system are:

- The system components were simulated under steady-state conditions.
- Potential and kinetic energies are neglected.
- H_2O and CO_2 are separated completely by the water separator.
- The heat loss from system components is neglected.

3.1. Thermodynamic modeling

3.1.1. Energy evaluation

The energy analysis of each system is used to determine how energy is converted from one form to another within the system, and how this affects the temperature, pressure, mass, and other properties of the system. Energy analysis is a fundamental aspect of the field of thermodynamics, which focuses on the relationships between energy, heat, and work. The basic premise of energy analysis in thermodynamics is the principle of conservation of energy, which states that energy cannot be created or destroyed, but can only be transformed from one form to another. The energy analysis as the base of the first law of thermodynamics is applied for each sub-system in the following sub-sections.

3.1.1.1. RO desalination unit. Typically, in an RO desalination unit, seawater undergoes a pre-treatment step before entering the main RO system. The feed flow rate can be calculated by using the recovery ratio (RR) and the mass flow rate of desalinated water [m^3/h].

$$M_{feed} = \frac{M_{permeate}}{RR} \tag{1}$$

The salt concentrations of rejected brine and desalinated water, can be calculated through Eqs. (2) and (3):

$$X_{brine} = \frac{M_{feed}X_{feed} - M_{permeate}X_{permeate}}{M_{brine}} \tag{2}$$

$$X_{permeate} = X_{feed}(1 - SR) \tag{3}$$

where SR is salt rejection percentage and X is salt concentration [kg/

m^3]. The temperature correction factor (TCF) is calculated as follows (Alirahmi et al., 2020):

$$TCF = \exp\left(2700\left(\frac{1}{T_{RO}} - \frac{1}{298}\right)\right) \tag{4}$$

The salt permeability (k_s) and membrane water permeability (k_w) is (Nafey and Sharaf, 2010):

$$k_s = FF \times TCF \times 4.72 \times 10^{-7}\left(0.06201 - \left(5.31 \times 10^{-5} \times T_{RO}\right)\right) \tag{5}$$

$$k_w = \frac{6.84 \times 10^{-8}(18.6865 - (0.177X_{brine}))}{T_{RO}} \tag{6}$$

where FF is fouling factor and it is assumed to be 0.85 (Nafey and Sharaf, 2010). The net osmotic pressure across the membrane and average osmotic pressure on the feed side are presented as follow:

$$P_{net,RO} = P_{av,RO} - P_{permeate} \tag{7}$$

$$P_{av,RO} = 0.5\left(P_{feed} - P_{brine}\right) \tag{8}$$

where $P_{permeate}$, P_{feed} and P_{brine} are osmotic pressure for desalinated product side, feed side and brine side, respectively and calculated as follow:

$$P_{permeate} = 75.84X_{permeate} \tag{9}$$

$$P_{feed} = 75.84X_{feed} \tag{10}$$

$$P_{brine} = 75.84X_{brine} \tag{11}$$

Finally, the required power input to high-pressure pump and net pressure difference through the membrane is estimated by the following equations:

$$\dot{W}_{HP} = \frac{1000 \times \dot{m}_{feed} \times \Delta P}{3600 \times \rho_{feed} \times \eta_P} \tag{12}$$

$$\Delta P = \left(\frac{\dot{m}_{permeate}}{3600 \times TCF \times FF \times A_e \times n_e \times n_v \times k_w}\right) + P_{net,RO} \tag{13}$$

The relevant parameters for the RO modeling are summarized in Table 1.

3.1.1.2. PEM electrolyzer. Green hydrogen is typically produced by the electrolysis of water using renewable energy. PEM electrolysis has gained popularity recently due to its favorable performance and low maintenance costs. The excess power from offshore wind turbine is to supply the required electricity for the electrolysis process. The PEM electrolyzer produces hydrogen based on the following chemical reaction:

$$\text{Anode reaction}: H_2O \rightarrow 2H^+ + \frac{1}{2}O_2 + 2e^- \tag{14}$$

$$\text{Cathode reaction}: 2H^+ + 2e^- \rightarrow H_2 \tag{15}$$

$$\text{Overall reaction}: H_2O + \text{energy} \rightarrow H_2 + \frac{1}{2}O_2 \tag{16}$$

The produced hydrogen and oxygen flow rate can be calculated by:

Table 1
Input parameters for the RO modeling (Nafey and Sharaf, 2010).

Variable	Value
Feed pressure (State 1), (P_{feed})	6700 [kPa]
Fouling factor (FF)	0.85
Number of elements (n_e)	7
Number of pressure vessels (n_v)	42
Recovery ratio (RR)	0.3

$$\dot{N}_{H_2,out} = \frac{J}{2F} \tag{17}$$

$$\dot{N}_{O_2,out} = \frac{J}{4F} \tag{18}$$

here F and J are Faraday constant and current density. The equation below can be used to calculate the power consumption of a PEM electrolyzer.

$$\dot{W}_{PEM} = JV \tag{19}$$

where V is PEM electrolyzer voltage for each cell and determined by:

$$V = V_0 + V_{act,c} + V_{act,a} + V_{ohm} + V_{conc} \tag{20}$$

where $V_{act,c}$ and $V_{act,a}$ are the activation overpotentials of the cathode and anode respectively and V_{ohm} is the ohmic overpotential. Since in this work, the current density is below 10,000 [A/m^2], the concentration overpotentials (V_{conc}) can be neglected. V_0 is the reversible potential and is calculated using the Nernst equation (Abdin et al., 2015):

$$V_0 = 1.229 - 0.85 \times 10^{-3}(T_{PEM} - T_0) + \frac{RT_{PEM}}{2F}\ln\frac{P_{O_2}^{0.5}P_{H_2}}{a_{H_2O}} \tag{21}$$

where a_{H_2O} is equal 1 for liquid water (Abdin et al., 2015). The activation overpotentials of the anode and cathode can be expressed as:

$$V_{act,i} = \frac{RT}{F}\sinh^{-1}\left(\frac{J}{2J_{0,i}}\right), i = a, c \tag{22}$$

In Eq. (23) $J_{0,i}$ is the exchange current density, which is a critical parameter for the calculation of the activation overpotential.

$$J_{0,i} = J_i^{ref}\exp\left(-\frac{E_{act,i}}{RT}\right), i = a, c \tag{23}$$

where j_i^{ref} and $E_{act,i}$ are pre-exponential factor and activation energy. Finally, ohmic voltage is defined as the following equations:

$$V_{ohm} = JR_{PEM} \tag{24}$$

$$R_{PEM} = \int_0^L \frac{dx}{\sigma[\lambda(x)]} \tag{25}$$

$$\sigma[\lambda(x)] = [0.5139\lambda(x) - 0.326]\exp\left[1268\left(\frac{1}{303} - \frac{1}{T_{PEM}}\right)\right] \tag{26}$$

$$\lambda(x) = \frac{\lambda_a - \lambda_c}{L}x + \lambda_c \tag{27}$$

where R_{PEM} and λ are overall ohmic resistance and water contents. The input parameters for the PEM electrolyzer are given in Table 2.

3.1.1.3. Methanation unit. Lagrange's method of undetermined multipliers is used in this study to determine the equilibrium state of the chemical process. In order to find the chemical reaction equilibrium, this algebraic solution minimizes the Gibbs free energy, and it is fast and

Table 2
Parameters employed in PEM electrolyzer modeling (Dincer et al., 2017a).

Variable	Value
PEM temperature (T_{PEM})	353 [K]
Activation voltage of the anode ($E_{act,a}$)	76,000[J/mol]
Activation voltage of the cathode ($E_{act,c}$)	18,000[J/mol]
Water contents at the anode (λ_a)	14
Water contents at the cathode (λ_c)	10
Membrane thickness (L)	100 [μm]
Current density of the anode (j_a^{ref})	1.7×10^5 [A/m^2]
Current density of the cathode (j_c^{ref})	4.6×10^3 [A/m^2]

accurate. As long as temperature and pressure remain constant, the Gibbs free energy total derivative must equal zero, which means:

$$dG = \sum_{i=1}^{C}\left[\mu_i + \sum_{j=1}^{E}\lambda_i\left(\frac{\partial\psi}{\partial n_i}\right)_{j\neq i}\right] = 0 \tag{28}$$

where C and E correspondingly represent number of compounds and elements involved in the reaction and n is the number of the ith compound moles. The chemical potential of every element for an ideal gas mixture presented as follow (Jalili et al., 2023):

$$\mu_i = T_{MU}\overline{S}_i^0 + RT_{MU} \times \ln\frac{y_i \times P_{MU}}{P_0} \tag{29}$$

where $\overline{S}_i^0$ is the molar specific entropy, R is the universal gas constant, T_{MU} is the temperatures of Sabatier reactor and y is the mole fraction. If all of the summing terms are zero, then Eq. (28) is satisfied, as follows.

$$\mu_i + \sum_{j=1}^{E}\lambda_i\left(\frac{\partial\psi}{\partial n_i}\right)_{j\neq i} = 0, \text{for } i = 1, ..C \tag{30}$$

where, ψ is the element balance function, which is calculated as follows:

$$\psi_j = \sum_{j=1}^{C} n_i e_{i,j} - E_{0,j} = 0, \text{for } j = 1, ..E \tag{31}$$

where, $e_{i,j}$ and $E_{0,j}$ and are the number of the jth element moles that exists in 1 mol of the ith compound and the number of the initial moles of each element present in the reaction, respectively.

The main Sabatier reaction that converts carbon dioxide into methane can be written as follow:

$$4H_2 + CO_2 \rightleftharpoons CH_4 + 2H_2O \Rrightarrow \text{Sabatier reaction} \tag{32}$$

The following side reactions may also occur in the methanation reactor (Beyrami et al., 2022):

$$3H_2 + CO \rightleftharpoons CH_4 + H_2O \Rrightarrow \text{Methanation reaction} \tag{33}$$

$$H_2O + CO \rightleftharpoons CO_2 + H_2 \Rrightarrow \text{Water gas shift reaction} \tag{34}$$

$$CO + H_2 \rightleftharpoons C + H_2O \Rrightarrow \text{Carbon monoxide reduction} \tag{35}$$

$$CO_2 + 2H_2 \rightleftharpoons C + 2H_2O \Rrightarrow \text{Carbon dioxide reduction} \tag{36}$$

Finally, the following equations can be used to calculate the equilibrium conversion of CO_2 and the methane yield from the equilibrium composition:

$$CO_2\ conversion\ [\%] = \frac{CO_{2,in} - CO_{2,out}}{CO_{2,in}} \times 100 \tag{37}$$

$$CH_4\ generation\ [\%] = \frac{CH_{4,out}}{CO_{2,in}} \times 100 \tag{38}$$

3.1.2. Exergy evaluation

Exergy analysis is a powerful tool for evaluating the performance of a thermodynamic system. Unlike traditional energy analysis, exergy analysis takes into account the quality and availability of energy within the system, allowing for a more comprehensive analysis of its efficiency and performance. Analyzing the exergy destruction and irreversibility of each component allows for a more accurate assessment of the system's efficiency and identification of components that require improvement. This information is valuable for optimizing the design and operation of energy systems and increasing their overall efficiency. Overall, exergy analysis is an essential tool for optimizing the design and operation of energy systems and promoting sustainable energy production and consumption.

In general, exergy has four main parts: physical, chemical, potential, and kinetic. Potential exergy is the exergy stored in an object due to its position in a gravitational field, while kinetic exergy is the exergy stored in an object due to its motion. Since elevation and velocity are assumed to be zero or low in most of the energy system, these two components are usually ignored (Ahmadi et al., 2011). So, the exergy rate can be expressed as:

$$\dot{E}x = \dot{E}x_{ph} + \dot{E}x_{ch} \tag{39}$$

And the exergy balance of each component is written as follows (Nabat et al., 2020):

$$x_Q + \sum_{i=1}^{n}\dot{E}x_{in,i} = \sum_{i=1}^{n}\dot{E}x_{out,i} + \dot{E}x_W + \dot{E}x_D \tag{40}$$

$$\dot{E}x_W = \dot{W} \tag{41}$$

where Q, W, and D subscripts refer to heat, work, and destruction.

3.1.2.1. Physical exergy. Physical exergy, also known as available energy or work potential, is a measure of the maximum useful work that can be extracted from a system as it comes into equilibrium with its surroundings. Several factors influence the physical exergy, including temperature, pressure, and the specific enthalpy and entropy. The physical exergy rate can be calculated using the following equation (Alirahmi et al., 2022):

$$\dot{E}x_{ph} = \sum_{i=1}^{n}\dot{m}_i((h_i - h_0) - T_0(s_i - s_0)) \tag{42}$$

3.1.2.2. Chemical exergy. During a chemical reaction, chemical exergy represents the maximum amount of work a substance can produce. The concept of chemical exergy is useful in a variety of fields, including thermodynamics, energy conversion, and process engineering. The molar chemical exergy for an ideal gas mixture is defined as follows (Dincer et al., 2017b; Ebrahimi-Moghadam et al., 2020):

$$\overline{ex}_{ch} = \sum_{i=1}^{n} x_i\overline{ex}_{ch}^{i} + RT_0\sum_{i=1}^{n} x_i\ ln(x_i) \tag{43}$$

where, $\overline{ex}_{ch}^{i}$ is the standard exergy of the constituents and x_i is the mole fraction of the ith component.

3.2. Performance evaluation metrics

Efficiency is an objective indicator for evaluating and comparing the performance of different systems. Both energy and exergy efficiencies can be used for this purpose. However, exergy efficiency is more meaningful as it takes into account thermodynamic inefficiencies that may not be reflected in energy efficiency alone. The exergy efficiency of the proposed system can be calculated by the following equation.

$$\eta_{ex} = \frac{\dot{W}_{net} + \dot{E}x_{18} + \dot{E}x_{Heating}}{\dot{E}x_{Wind\ turbine}} \tag{44}$$

where, $\dot{E}x_{Heating}$ is the thermal exergy rate and can be expressed by the following equation (Rejeb et al., 2022):

$$\dot{E}x_{Heating} = \left(1 - \frac{T_0}{T}\right)\dot{Q}_{Heating} \tag{45}$$

4. Validation

The proposed integrated system is a novel concept that has not been reported in the open literature. Therefore, the acquired data from each subsystem of this model is validated individually with the relevant studies. The proposed system consists of three main subsystems, namely Allam cycle, PEM and methanation unit. The comparison between this study and previously published study on Allam cycle is presented in Table 3. It should be noted that the previous studies employed an air separator and did not consider the use of oxygen from an electrolyzer. Despite that, the resulting discrepancy does not exceed 3.9%.

Table 3
Comparison of the model with the reported data in Allam et al. (2017).

Parameter	Allam et al. (2017)	Present study	Relative Difference [%]
Net output power (including ASU) [MW]	359 (303)	365	1.67%
NG thermal input [MW]	511	511	Input
O_2 consumption [MT/day]	3555	3688	3.74%
Turbine outlet flow [kg/s]	923	920.7	0.25%
GT inlet condition	300 bar/ 1158 °C	300 bar/ 1158 °C	Input
GT outlet condition	30 bar/ 727 °C	30 bar/ 752.4 °C	3.44%
ASU power [MW]	56	–	–
CO_2 compression power [MW]	77	80	3.9%

The validation results of the PEM and methanation unit are also reported in Fig. 2. The PEM electrolyzer and methanation unit models are validated against the experiment data from Ioroi et al., (2002) and model data from Mendoza-Hernandez et al., (2019), respectively. As can be see, the data are in good agreement.

5. Results and discussion

For evaluating the system's operation, thermodynamic and exergy analyses are presented in this section. In order to obtain a comprehensive view of the thermodynamic performance of the system, the energy and mass balance equations are applied. Tables 4 and 5 provide the thermodynamic characteristics and molar percentages of the state points of the proposed IES for the case with a storage ratio of 50%.

Table 4
Thermodynamic results of the state points.

State no.	T(°C)	P(Bar)	ṁ(kg/s)
1	10	1.013	2.032
2	10	1.013	0.6096
3	37.23	1.013	1.779
4	30.28	1.013	2.389
5	30.28	1.013	2.389
6	30.31	10	2.389
7	80	10	0.2673
8	80	10	2.122
9	80	10	1.061
10	80	10	1.061
11	210.9	27.12	1.061
12	25	10	1.459
13	300	10	1.726
14	300	10	1.726
15	41	10	1.726
16	41	10	1.17
17	41	10	0.5566
18	196.9	54.77	0.2783
19	196.9	300	0.2783
20	6.85	27.12	1.061
21	138.8	300	1.061
22	1150	294	22.97
23	779.2	30	22.97
24	247.9	28.5	22.97
25	30	27.08	22.97
26	30	27.08	0.6096
27	30	27.08	22.36
28	30	27.08	0.7295
29	30	27.08	21.63
30	114.5	73.77	21.63
31	30	73.77	21.63
32	72.51	300	21.63
33	701.5	300	21.63

5.1. Parametric study

Parametric study is a method of design exploration that uses mathematical models to explore the relationships between design parameters and the results of a simulation. By using this tool, designers are able to quickly visualize the effects of changes on a system and improve the efficiency of the design process. Parametric study can also be used to identify the design parameters that have the greatest impact on performance, allowing designers to focus on developing solutions that optimize the most critical aspects of a system.

The impact of temperature and pressure of methanation unit on the system performance is illustrated in Fig. 3. The figure shows that the highest mole fraction of products (H_2O and CH_4) is achieved at lower temperatures, indicating that the Sabatier reaction is more favorable at lower temperatures. Conversely, at higher temperatures, CH_4 production decreases while CO generation increases. As a result, more hydrogen is required for the Sabatier reaction, and more electrical power is required for the electrolyzer as the temperature rises. The system's efficiency remains relatively high within the temperature range of 200–300 °C, as shown in Fig. 3a, but decreases as the temperature rises. On the other hand, as the temperature decreases, the reaction rate decreases and the volume of the methanation unit increases.

Increasing the pressure can enhance exergy efficiency, as depicted in Fig. 3a, but it can also increase the stress on the reactors, necessitating thicker walls and increasing the reactor cost. According to Jürgensen et al. (2015), it is commonly advised to operate the reactor within a temperature range from 250 to 500 °C, along with a pressure of 10 bar to achieve a high methane yield. Based on the results illustrated in Fig. 3, it is suggested that the operating conditions should be set around 300 °C with a pressure of 10 bar.

Fig. 4 depicts the relationship between current density, electrolyzer power consumption and the exergy efficiency at different temperatures. The electricity consumption of the electrolyzer exhibits a steep increase up to a current density of 200 (A/m^2) and a gradual increase beyond 200 (A/m^2). Generally, the exergy efficiency of the system decreases with

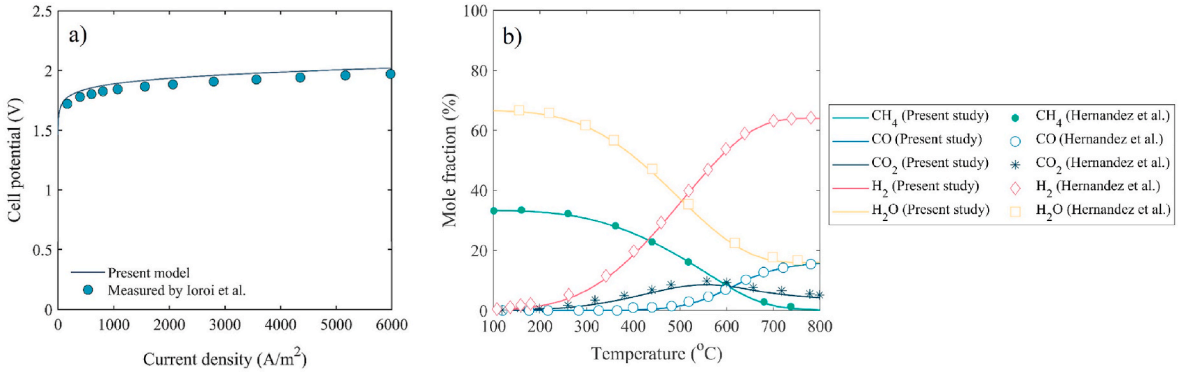

Fig. 2. Validation of the model for a) PEM electrolyzer (Ioroi et al., 2002), b) methanation unit (Mendoza-Hernandez et al., 2019).

Table 5
Molar percentages of the state points.

State no.	Molar percentage (%)					
	CH_4	H_2O	CO	CO_2	H_2	O_2
1	–	–	–	–	–	–
2	–	100	–	–	–	–
3	–	100	–	–	–	–
4	–	100	–	–	–	–
5	–	100	–	–	–	–
6	–	100	–	–	–	–
7	–	–	–	–	100	–
8	–	–	–	–	–	100
9	–	–	–	–	–	100
10	–	–	–	–	–	100
11	–	–	–	–	–	100
12	–	–	–	100	–	–
13	–	–	–	20	80	–
14	32.2	64.39	0.007	2.72	0.683	–
15	32.2	64.39	0.007	2.72	0.683	–
16	–	100	–	–	–	–
17	90.43	–	0.002	7.658	1.91	–
18	90.43	–	0.002	7.658	1.91	–
19	90.43	–	0.002	7.658	1.91	–
20	–	–	–	–	–	100
21	–	–	–	–	–	100
22	–	6.24	–	93.76	–	–
23	–	6.24	–	93.76	–	–
24	–	6.24	–	93.76	–	–
25	–	6.24	–	93.76	–	–
26	–	100	–	–	–	–
27	–	–	–	100	–	–
28	–	–	–	100	–	–
29	–	–	–	100	–	–
30	–	–	–	100	–	–
31	–	–	–	100	–	–
32	–	–	–	100	–	–
33	–	–	–	100	–	–

increasing current density since the overall input energy increases at a higher rate compared to output energy (generated hydrogen).

Although exergy efficiency favors lower current density, a minimum current density is required for a PEM electrolyzer to operate efficiently and produce hydrogen at a reasonable rate. There are some disadvantages associated with operating at extremely low current densities. One major disadvantage is that the rate of hydrogen production is relatively low, indicating that the electrolyzer should be bigger to produce the same amount of hydrogen, which can be inefficient and may not meet the demands of offshore applications. Additionally, operating at extremely low current densities can also result in poor gas diffusion and inefficient use of the catalysts, leading to decreased electrolyzer performance and durability. Therefore, while it is important to operate at an appropriate current density to optimize the performance of a PEM electrolyzer, operating at low current densities can negatively impact operability, durability, and reliability of the electrolyzer. On the other hand, it is important to note that while a higher current density may increase the rate of hydrogen production, it can also lead to greater energy losses due to heat generation and damage to the electrolyzer components over time. Therefore, it is crucial to trade-off the current density with other operating parameters such as temperature, pressure, and flow rate to optimize the performance and longevity of the PEM electrolyzer.

Based on Fig. 4, higher temperatures are preferable for the better efficiency of the system, yet the process temperature should not be too high because liquid water is required for the ionic conductivity of the electrolyte membrane and water boils at high temperatures and increasing temperature further rupture the membrane.

The combustor outlet temperature (or inlet temperature of the GT) is one of the most important parameters in the Allam cycle. Fig. 5 shows the impact of combustor outlet temperature on the system exergy efficiency and power output. The efficiency and output power of the Allam cycle (for the scenario of 50% storage ratio) increases as the combustor outlet temperature changing from 700 to 1250 °C. In order to maintain the Allam cycle in optimum performance and efficiency, the combustor outlet temperature needs to be kept in a certain range, which is determined by the thermodynamic properties of the working fluid and the materials. An extremely high temperature is not plausible considering the limitations of turbine materials and the increased heat load of the heat exchanger on the turbine exhaust stream, which results in a larger heat exchanger.

Fig. 6 depicts the impact of turbine inlet pressure on exergy efficiency and Allam cycle output power in various storage ratio scenarios. It is apparent that system efficiency and Allam cycle output power increase as the GT inlet pressure rises and this trend is consistent across all storage ratio scenarios. Therefore, it can be inferred that the optimal GT inlet pressure should be more than 300 bar.

Based on the findings of this study, a maximum pressure within the range of 300–350 bar is recommended since the slope of the efficiency curve decreases after 350 bar and operational and equipment cost beyond 350 bar increases.

Fig. 7 shows the GT outlet and inlet pressure contour versus the system efficiency. It is better to evaluate outlet pressure regarding the inlet pressure since maximum and minimum pressures are correlated in the Allam cycle. By increasing the maximum pressure, the turbine produces more power, but the pump and compressor consume more power as well. Also, as minimum pressure increases, the amount of power produced by the turbine and the amount of power consumed by the pump and compressor decreases. Nevertheless, the increase in turbine power dominates compressor power consumption at lower pressure

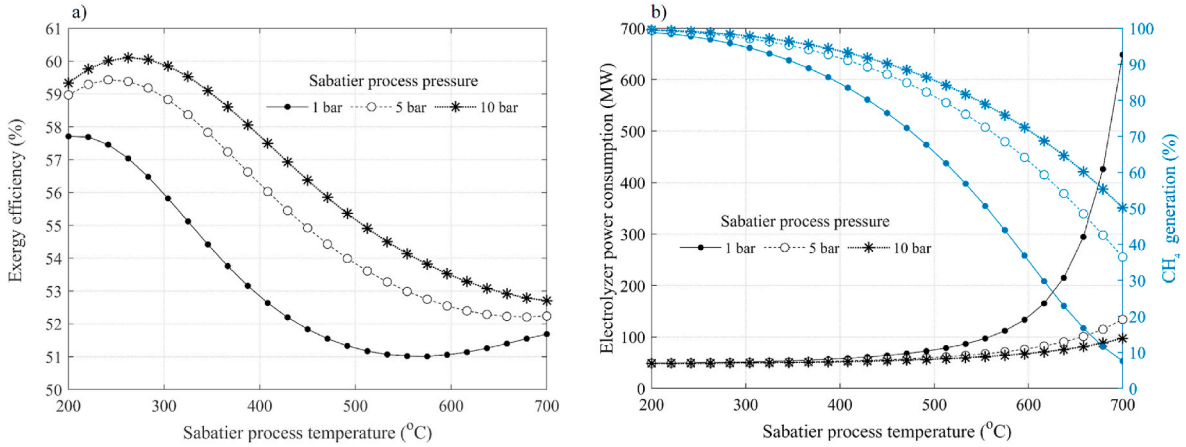

Fig. 3. Impact of temperature and pressure methanation unit on the system's performance.

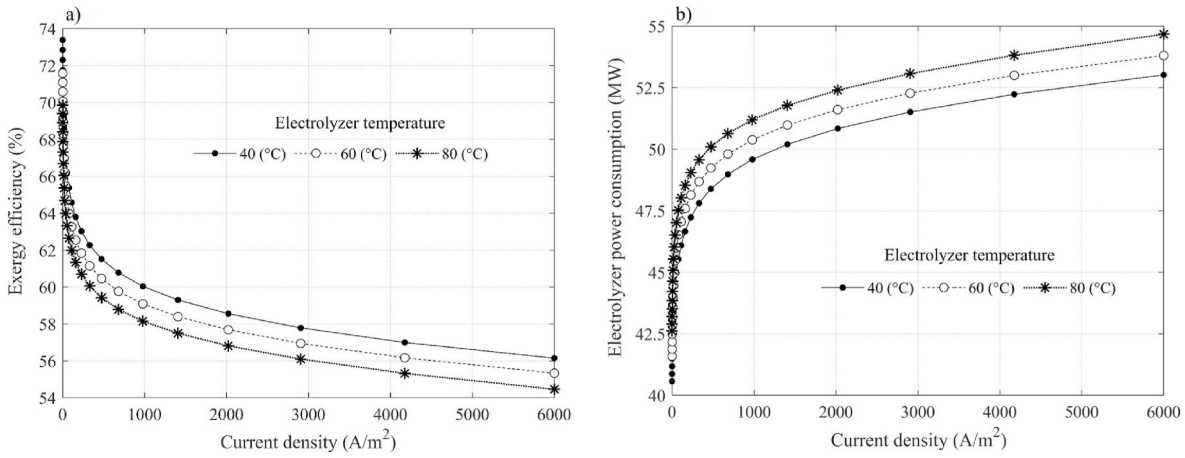

Fig. 4. Impact of electrolyzer current density on the system's performance.

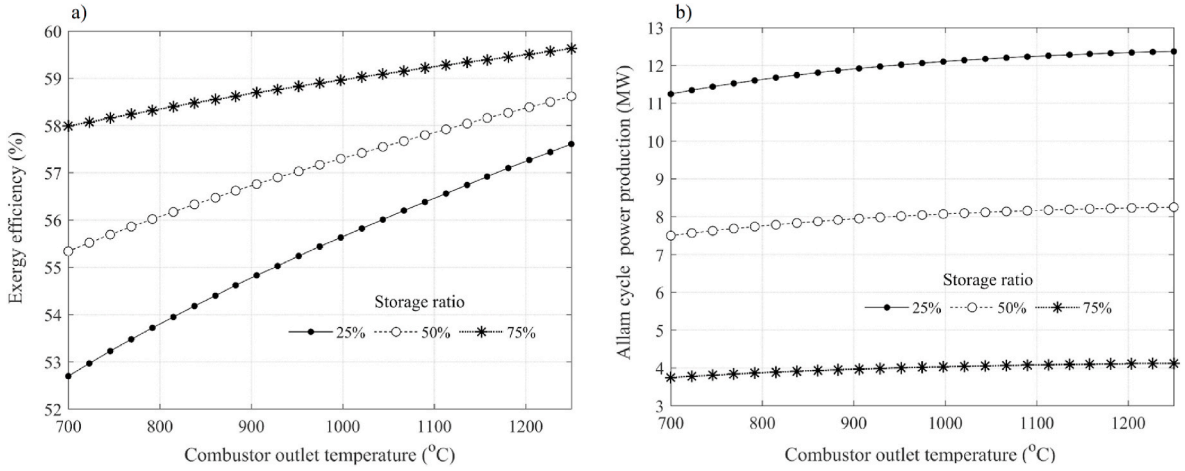

Fig. 5. Impact of combustor outlet temperature on the system's performance.

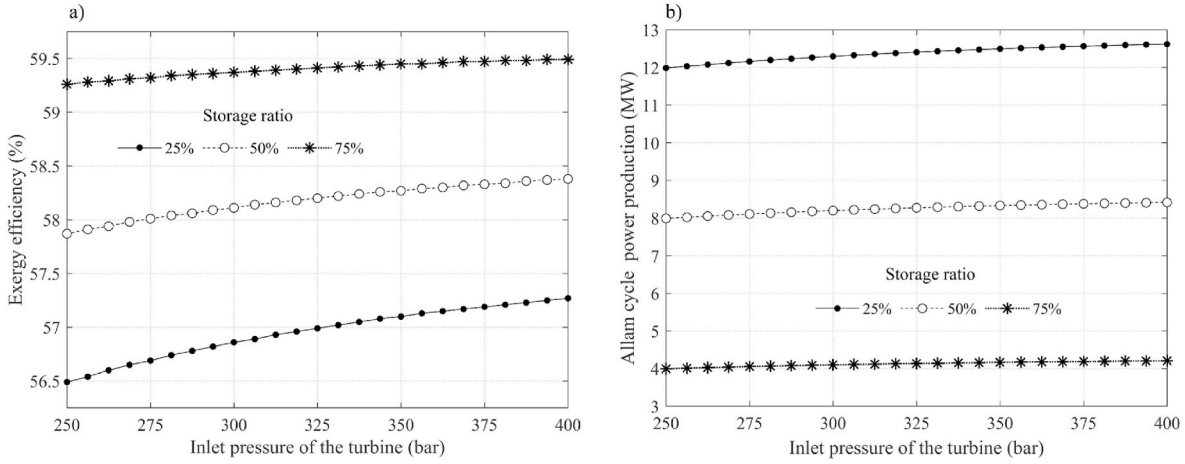

Fig. 6. Impact of inlet pressure of the turbine on the system's performance.

ratios. However, by increasing the pressure ratio, this trend is vice versa. As shown in Fig. 7 increasing the GT outlet pressure leads to a rise in the system efficiency, peaking in the range of 25–35 bar and then declining. Therefore, it can be concluded that the thermodynamically optimal outlet pressure is in range of 25–35 bar.

5.2. Scenarios analysis

The key metrics of the integrated system under different scenarios are listed in Table 6, where the + sign means production and the – sign means consumption. When all the synthesized methane is burned in the Allam cycle, CO_2 cannot be net consumed, since the CO_2 generated in

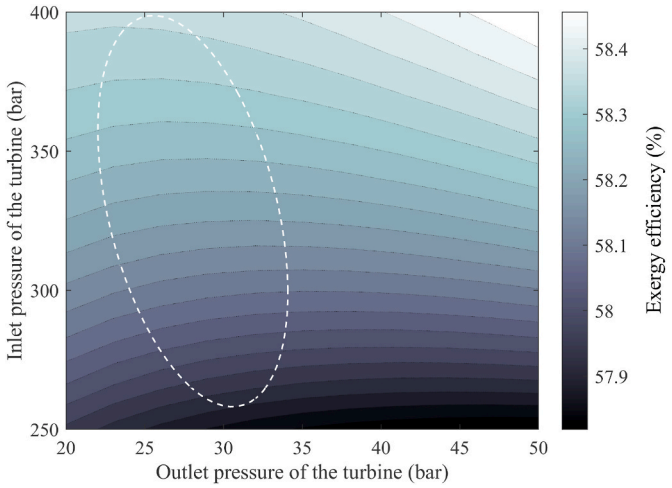

Fig. 7. Impact of inlet and outlet pressure of the turbine on the system's performance.

Table 6
Comparison of different scenarios under various storage ratio.

	Storage ratio				
	100%	75%	50%	25%	0%
Allam cycle power (MW)	0	4.1	8.2	12.3	16.4
Oxygen (kg/s)	+2.12	+1.59	+1.06	+0.53	~0
Methane (kg/s)	+0.556	+0.417	+0.278	+0.139	0
Carbon dioxide (kg/s)	−1.46	−1.09	−0.73	−0.36	0

the Allam cycle matches the CO_2 needed as input to the methanation reactor. On the contrary, if all the synthesized methane is exported to shore or stored in the reservoir, the Allam cycle can be eliminated from the system. When all the synthesized methane is burned in the Allam cycle, 51.34 MW of electricity from offshore wind farms can be transformed into 16.4 MW of dispatchable electricity from Allam cycle. In this scenario, the integrated system can be regarded as an energy storage system, where the round-trip efficiency is about 32%.

The Grassmann diagrams are presented and compared in Fig. 8 to evaluate the performance of the system in three different scenarios, namely 25%, 50%, and 75% storage ratio. As can be deduced, the efficiency of the electrolyzer, methanation unit, and Allam cycle is 63%, 74%, and 67%, respectively. However, due to the efficient utilization of O_2 and CO_2, the overall efficiency of the system can reach around 60%. Also, considering that the Allam cycle causes some exergy degradation, the system exergy efficiency can be improved by consuming less methane in the Allam cycle, but at the cost of generating less electricity.

Additionally, the performance of the integrated system is evaluated from the perspective of exergy. In general, improving the efficiency of individual equipment is limited in its impact, and greater gains can be achieved by identifying and reducing energy losses throughout the overall system exergy flow. The Grassmann diagram in Fig. 9 illustrates the exergy flow of the scenario with a storage ratio of 50%.

The process begins with the electrolyzer, which combines water and electricity to produce hydrogen and oxygen. However, 36% of the input electricity is wasted, leaving hydrogen as the primary useful output exergy due to its high chemical exergy. The resulting hydrogen with an exergy of 32.06 MW is then fed into the methanation unit together with CO_2, producing high-temperature heat in the methanation process, which should be cooled down before separation and pressurizing. These exergy sources can be harnessed to improve the efficiency of the system process. Overall, approximately 55% of the electrical energy utilized for electrolysis is stored as chemical energy in the form of methane. Subsequently, 50% of the produced methane enters the methane pipeline and the rest is fed to the Allam cycle. The methane and oxygen enter the combustion chamber. Afterwards, the combustion products with high temperature and pressure drives the turbine, and 30% of the exergy is turned into electrical power through the expansion process. It could also be observed that the Allam cycle condenser has a high exergy destruction due to the high temperature difference between the streams of the condenser. Overall, out of 51.32 MW of system input electricity (plus 0.38 MW exergy from the CO_2 tank), 29.53 MW exergy is destroyed, and 12.16, 8.19, and 1.61 MW are converted into chemical exergy, electrical energy, and thermal exergy, respectively.

In the end, Fig. 10 illustrates the chord diagram of the exergy destruction rate, which represents the inter-relationship between the overall exergy destruction and the contribution of each subsystem to it. The size of the arc is proportional to the amount of energy destroyed by the unit. Among 29.53 MW of exergy destruction, the electrolyzer, methanation unit, and the Allam cycle, account for 62.2%, 24.1%, and 13.2%, respectively. Also, the exergy destruction of the RO unit is very low compared to main units of the system and it is lumped into the exergy destruction of other components as illustrated in Fig. 10. In addition, any improvement to the electrolyzer unit would result in a significant improvement in overall system performance.

6. Conclusions

In order to repurpose offshore O&G platforms by integration with offshore wind farms, a novel integrated energy system was presented in this study. The synergies between the offshore O&G platform and the offshore wind farms are explored. The cross-sector integration can lead to substantial benefits in terms of energy efficiency, economy and environment. The novel integrated energy system provides a promising solution for decommissioning offshore O&G platforms at the end of production by 2050. The simulation is performed based on 45 ton/day of synthesized methane, which represents about 1% of the total daily natural gas consumption in Denmark. The energy and exergy analysis is performed based on the simulation results. The parametric analysis examined both the subsystem and the integrated system performance. Finally, the Grassmaan and Chord diagrams were represented to investigate the system's performance from exergy perspective. The main results can be summarized as follows:

- The parametric analysis shows that the temperature of the methanation unit and the current density of the electrolyzer had the highest impact on system performance.
- According to the parametric analysis, the methanation unit temperature and pressure should be kept around 300 °C with a pressure of 10 bar.
- The exergy efficiency of the PEM electrolyzer, methanation unit, and Allam cycle were determined to be 63%, 74%, and 67%, respectively, while the overall exergy efficiency of the integrated system was found to be 60%.
- Due to the presence of chemical reactions, the PEM electrolyzer and the methanation unit had the most exergy destruction.

From a thermodynamic perspective, the findings of this study suggest that the novel integrated system holds promise as a viable solution for repurposing the offshore platform beyond 2050. The overall efficiency can be further improved if optimization is performed. Also, a trade-off between efficiency and material limitations must be considered when designing the Allam cycle. Further research is needed to optimize the combustor outlet temperature for maximum efficiency while maintaining safe and sustainable operation. However, there are some practical challenges in the system, such as the unsteady state condition of the electrolyzer and the methanation unit. In future work, process optimization, techno-economic analysis, unsteady behavior of the electrolyzer and methanation unit, and the impact of water quality on the electrolyzer performance should be investigated.

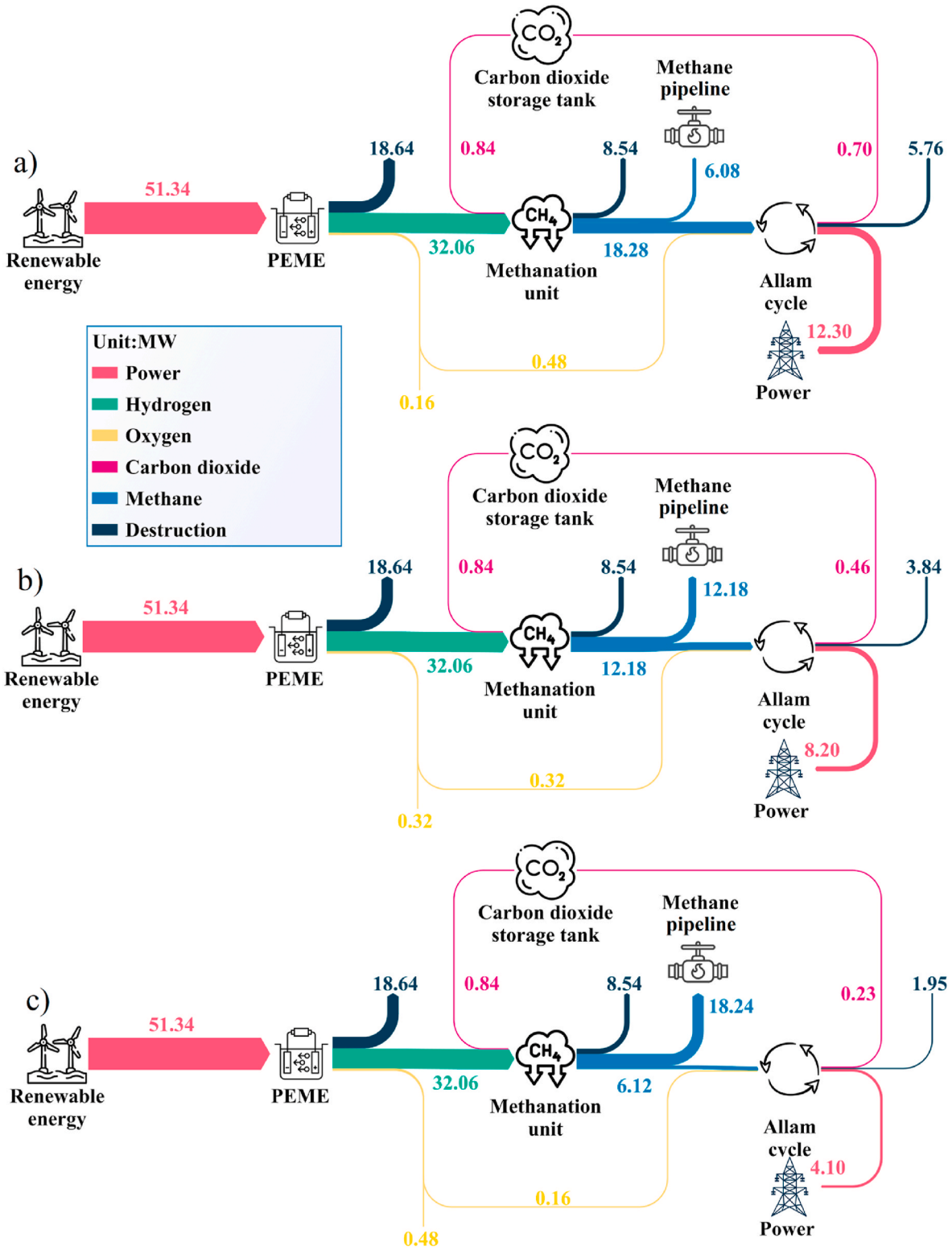

Fig. 8. The Grassmann diagrams of the integrated energy system under different scenarios. a) storage ratio is 25%. b) storage ratio is 50%. c) storage ratio is 75%.

CRediT authorship contribution statement

Seyed Mojtaba Alirahmi: Methodology, Software, Formal analysis, Writing – original draft. **Alessandro Perrucci:** Investigation, Validation. **Marco Maschietti:** Investigation, Validation, Writing – review & editing. **Meng Qi:** Validation, Writing – review & editing. **Emre Gençer:** Validation, Writing – review & editing. **Gürkan Sin:** Methodology, Supervision. **Haoshui Yu:** Conceptualization, Methodology, Supervision.

Declaration of competing interest

The authors declare that they have no known competing financial interests or personal relationships that could have appeared to influence

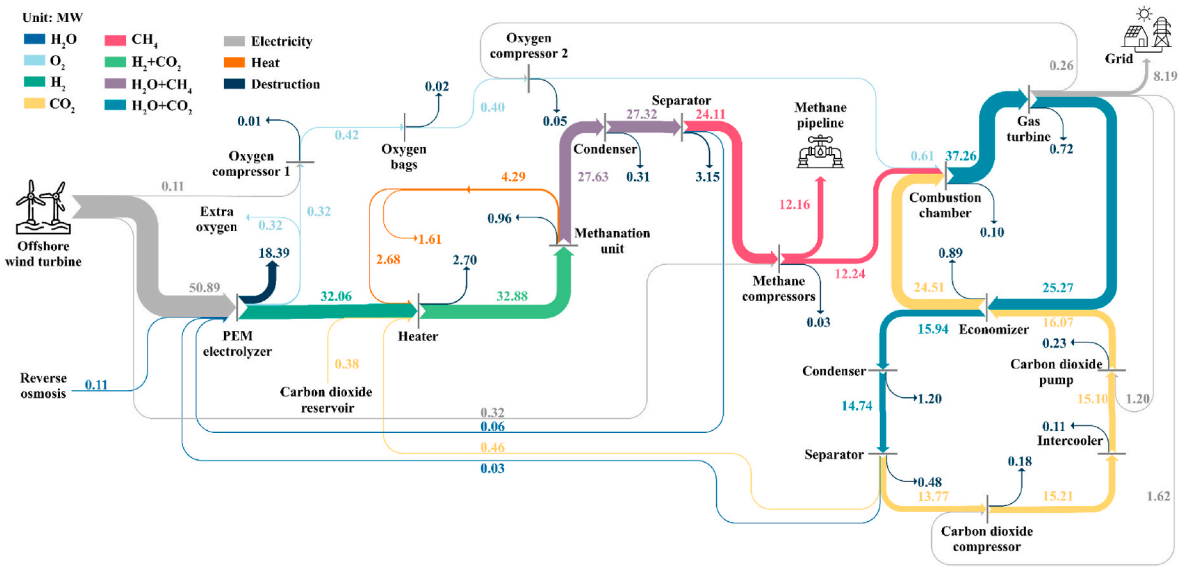

Fig. 9. The Grassmann diagram of the proposed system for the scenario with a storage ratio of 50%.

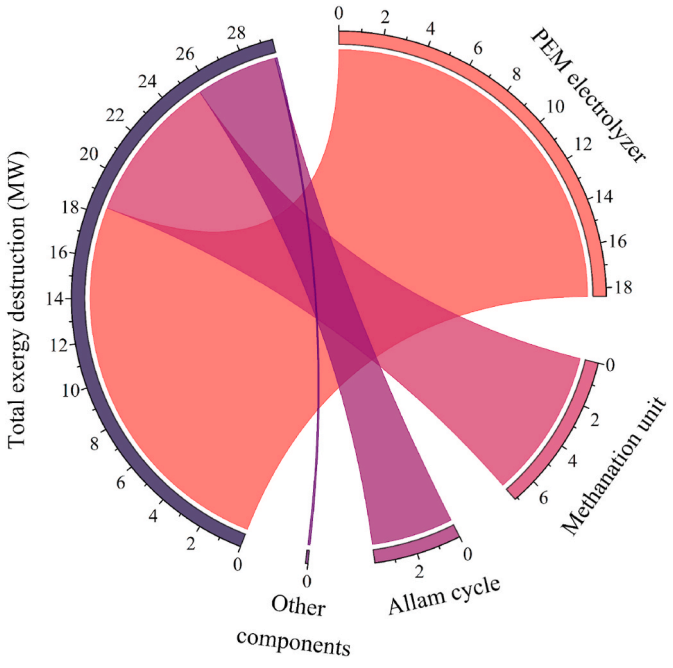

Fig. 10. The chord diagram of the exergy destruction for each subsystem.

the work reported in this paper.

Data availability

Data will be made available on request.

Acknowledgement

The authors would like to express their gratitude for the financial support provided by the Danish Offshore Technology Centre's Radical Innovation Sprint (RIS) project. Additionally, they would like to extend their appreciation to Karen Guldbæk Schmidt for her valuable input and insightful discussions during the project.

References

Abdin, Z., Webb, C.J., Gray, E.M., 2015. Modelling and simulation of a proton exchange membrane (PEM) electrolyser cell. Int. J. Hydrogen Energy 40, 13243–13257. https://doi.org/10.1016/j.ijhydene.2015.07.129.

Ahmadi, P., Dincer, I., Rosen, M.A., 2011. Exergy, exergoeconomic and environmental analyses and evolutionary algorithm based multi-objective optimization of combined cycle power plants. Energy 36, 5886–5898. https://doi.org/10.1016/j.energy.2011.08.034.

Alirahmi, S.M., Assareh, E., Arabkoohsar, A., Yu, H., Hosseini, S.M., Wang, X., 2022. Development and multi-criteria optimization of a solar thermal power plant integrated with PEM electrolyzer and thermoelectric generator. Int. J. Hydrogen Energy 47, 23919–23934. https://doi.org/10.1016/j.ijhydene.2022.05.196.

Alirahmi, S.M., Rahmani Dabbagh, S., Ahmadi, P., Wongwises, S., 2020. Multi-objective design optimization of a multi-generation energy system based on geothermal and solar energy. Energy Convers. Manag. 205, 112426 https://doi.org/10.1016/j.enconman.2019.112426.

Allam, R., Martin, S., Forrest, B., Fetvedt, J., Lu, X., Freed, D., Brown, G.W., Sasaki, T., Itoh, M., Manning, J., 2017. Demonstration of the Allam cycle: an update on the development status of a high efficiency supercritical carbon dioxide power process employing full carbon capture. Energy Proc. 114, 5948–5966. https://doi.org/10.1016/j.egypro.2017.03.1731.

Allam, R.J., Palmer, M.R., Brown, G.W., Fetvedt, J., Freed, D., Nomoto, H., Itoh, M., Okita, N., Jones, C., 2013. High efficiency and low cost of electricity generation from fossil fuels while eliminating atmospheric emissions, including carbon dioxide. Energy Proc. 37, 1135–1149. https://doi.org/10.1016/j.egypro.2013.05.211.

Bataille, C., Åhman, M., Neuhoff, K., Nilsson, L.J., Fischedick, M., Lechtenböhmer, S., Solano-Rodriquez, B., Denis-Ryan, A., Stiebert, S., Waisman, H., Sartor, O., Rahbar, S., 2018. A review of technology and policy deep decarbonization pathway options for making energy-intensive industry production consistent with the Paris Agreement. J. Clean. Prod. 187, 960–973. https://doi.org/10.1016/j.jclepro.2018.03.107.

Behzadi, A., Alirahmi, S.M., Yu, H., Sadrizadeh, S., 2023. An efficient renewable hybridization based on hydrogen storage for peak demand reduction: a rule-based energy control and optimization using machine learning techniques. J. Energy Storage 57, 106168. https://doi.org/10.1016/j.est.2022.106168.

Beyrami, J., Jalili, M., Ziyaei, M., Chitsaz, A., Rosen, M.A., 2022. A novel system for electricity and synthetic natural gas production from captured CO2: techno-economic evaluation and multi-objective optimization. J. CO2 Util. 63, 102116 https://doi.org/10.1016/j.jcou.2022.102116.

Bolland, O., Mathieu, P., 1998. Comparison of two CO2 removal options in combined cycle power plants. Energy Convers. Manag. 39, 1653–1663. https://doi.org/10.1016/S0196-8904(98)00078-8.

Cheung, B.C., Carriveau, R., Ting, D.S.K., 2014. Multi-objective optimization of an underwater compressed air energy storage system using genetic algorithm. Energy 74, 396–404. https://doi.org/10.1016/j.energy.2014.07.005.

Dincer, I., Rosen, M.A., Ahmadi, P., 2017a. Optimization of Energy Systems. Wiley. https://doi.org/10.1002/9781118894484.

Dincer, I., Rosen, M.A., Ahmadi, P., 2017b. Optimization of Energy Systems, Optimization of Energy Systems. John Wiley & Sons, Ltd, Chichester, UK. https://doi.org/10.1002/9781118894484.

Ebrahimi-Moghadam, A., Moghadam, A.J., Farzaneh-Gord, M., Aliakbari, K., 2020. Proposal and assessment of a novel combined heat and power system: energy, exergy, environmental and economic analysis. Energy Convers. Manag. 204, 112307 https://doi.org/10.1016/j.enconman.2019.112307.

Hermesmann, M., Grübel, K., Scherotzki, L., Müller, T.E., 2021. Promising pathways: the geographic and energetic potential of power-to-x technologies based on regeneratively obtained hydrogen. Renew. Sustain. Energy Rev. 138, 110644 https://doi.org/10.1016/j.rser.2020.110644.

Ioroi, T., Yasuda, K., Siroma, Z., Fujiwara, N., Miyazaki, Y., 2002. Thin film electrocatalyst layer for unitized regenerative polymer electrolyte fuel cells. J. Power Sources 112, 583–587. https://doi.org/10.1016/S0378-7753(02)00466-4.

Jalili, M., Ghazanfari Holagh, S., Chitsaz, A., Song, J., Markides, C.N., 2023. Electrolyzer cell-methanation/Sabatier reactors integration for power-to-gas energy storage: thermo-economic analysis and multi-objective optimization. Appl. Energy 329, 120268. https://doi.org/10.1016/j.apenergy.2022.120268.

Jürgensen, L., Ehimen, E.A., Born, J., Holm-Nielsen, J.B., 2015. Dynamic biogas upgrading based on the Sabatier process: thermodynamic and dynamic process simulation. Bioresour. Technol. 178, 323–329. https://doi.org/10.1016/j.biortech.2014.10.069.

Li, M., Luo, H., Zhou, S., Senthil Kumar, G.M., Guo, X., Law, T.C., Cao, S., 2022. State-of-the-art review of the flexibility and feasibility of emerging offshore and coastal ocean energy technologies in East and Southeast Asia. Renew. Sustain. Energy Rev. 162, 112404 https://doi.org/10.1016/j.rser.2022.112404.

Luo, Y., Wu, X.-Y., Shi, Y., Ghoniem, A.F., Cai, N., 2017. Exergy efficiency analysis of a power-to-methane system coupling water electrolysis and sabatier reaction. ECS Trans. 78, 2965–2973. https://doi.org/10.1149/07801.2965ecst.

Mathieu, P., Nihart, R., 1999. Zero-emission MATIANT cycle. J. Eng. Gas Turbines Power 121, 116–120. https://doi.org/10.1115/1.2816297.

McKenna, R., D'Andrea, M., González, M.G., 2021. Analysing long-term opportunities for offshore energy system integration in the Danish North Sea. Adv. Appl. Energy 4, 100067. https://doi.org/10.1016/j.adapen.2021.100067.

Mendoza-Hernandez, O.S., Shima, A., Matsumoto, H., Inoue, M., Abe, T., Matsuzaki, Y., Sone, Y., 2019. Exergy valorization of a water electrolyzer and CO2 hydrogenation tandem system for hydrogen and methane production. Sci. Rep. 9, 6470. https://doi.org/10.1038/s41598-019-42814-6.

Nabat, M.H., Zeynalian, M., Razmi, A.R., Arabkoohsar, A., Soltani, M., 2020. Energy, exergy, and economic analyses of an innovative energy storage system; liquid air energy storage (LAES) combined with high-temperature thermal energy storage (HTES). Energy Convers. Manag. 226, 113486 https://doi.org/10.1016/J.ENCONMAN.2020.113486.

Nafey, A.S., Sharaf, M.A., 2010. Combined solar organic Rankine cycle with reverse osmosis desalination process: energy, exergy, and cost evaluations. Renew. Energy 35, 2571–2580. https://doi.org/10.1016/j.renene.2010.03.034.

Pimm, A., Garvey, S.D., 2022. Underwater compressed air energy storage. In: Storing Energy. Elsevier, pp. 157–177. https://doi.org/10.1016/B978-0-12-824510-1.00025-8.

Rejeb, O., Alirahmi, S.M., Assareh, E., El Haj Assad, M., Jemni, A., Bettayeb, M., Ghenai, C., 2022. Innovative integrated solar powered polygeneration system for green Hydrogen, Oxygen, electricity and heat production. Energy Convers. Manag. 269, 116073 https://doi.org/10.1016/j.enconman.2022.116073.

Rogalev, A., Rogalev, N., Kindra, V., Komarov, I., Zlyvko, O., 2021. Research and development of the oxy-fuel combustion power cycles with CO2 recirculation. Energies 14, 2927. https://doi.org/10.3390/en14102927.

Sanz, W., Jericha, H., Moser, M., Heitmeir, F., 2005. Thermodynamic and economic investigation of an improved Graz cycle power plant for CO2 capture. J. Eng. Gas Turbines Power 127, 765–772. https://doi.org/10.1115/1.1850944.

Scaccabarozzi, R., Gatti, M., Martelli, E., 2016. Thermodynamic analysis and numerical optimization of the NET Power oxy-combustion cycle. Appl. Energy 178, 505–526. https://doi.org/10.1016/j.apenergy.2016.06.060.

Schaaf, T., Grünig, J., Schuster, M.R., Rothenfluh, T., Orth, A., 2014. Methanation of CO2 - storage of renewable energy in a gas distribution system. Energy. Sustain. Soc. 4, 2. https://doi.org/10.1186/s13705-014-0029-1.

Schrag, D.P., 2009. Storage of carbon dioxide in offshore sediments. Science 84 325, 1658–1659. https://doi.org/10.1126/science.1175750.

Shabani, H.R., Kalantar, M., Hajizadeh, A., 2022. Real-time transient instability detection in the power system with high DFIG-wind turbine penetration via transient energy. IEEE Syst. J. 16, 3013–3024. https://doi.org/10.1109/JSYST.2021.3079253.

Statista, 2022. Natural Gas Consumption in Denmark from 2005 to 2021. https://www.statista.com/statistics/703645/natural-gas-consumption-denmark/.

Thema, M., Bauer, F., Sterner, M., 2019. Power-to-Gas: electrolysis and methanation status review. Renew. Sustain. Energy Rev. 112, 775–787. https://doi.org/10.1016/j.rser.2019.06.030.

Toro, C., Sciubba, E., 2018. Sabatier based power-to-gas system: heat exchange network design and thermoeconomic analysis. Appl. Energy 229, 1181–1190. https://doi.org/10.1016/j.apenergy.2018.08.036.

Wang, Zhiwen, Ting, D.S.-K., Carriveau, R., Xiong, W., Wang, Zuwen, 2016. Design and thermodynamic analysis of a multi-level underwater compressed air energy storage system. J. Energy Storage 5, 203–211. https://doi.org/10.1016/j.est.2016.01.002.

Wu, X., Zhang, H., Yang, M., Jia, W., Qiu, Y., Lan, L., 2022. From the perspective of new technology of blending hydrogen into natural gas pipelines transmission: mechanism, experimental study, and suggestions for further work of hydrogen embrittlement in high-strength pipeline steels. Int. J. Hydrogen Energy 47, 8071–8090. https://doi.org/10.1016/j.ijhydene.2021.12.108.

Wulf, C., Zapp, P., Schreiber, A., 2020. Review of power-to-X demonstration projects in Europe. Front. Energy Res. 8 https://doi.org/10.3389/fenrg.2020.00191.

Xie, M., Chen, L., Wu, K., Liu, Z., Lin, J., Jiang, C., Xie, S., Zhao, Y., 2023. A novel peak shaving approach to improving load flexibility of the Allam cycle by integrating cold energy storage. J. Clean. Prod. 386, 135769 https://doi.org/10.1016/j.jclepro.2022.135769.

Zhixin, W., Chuanwen, J., Qian, A., Chengmin, W., 2009. The key technology of offshore wind farm and its new development in China. Renew. Sustain. Energy Rev. 13, 216–222. https://doi.org/10.1016/j.rser.2007.07.004.